

The effects of grain shape and frustration in a granular column near jamming

J.M. Luck¹ and A. Mehta²

¹ Institut de Physique Théorique, IPhT, CEA Saclay, and URA 2306, CNRS, 91191 Gif-sur-Yvette cedex, France.

e-mail: jean-marc.luck@cea.fr

² S.N. Bose National Centre for Basic Sciences, Block JD, Sector 3, Salt Lake, Calcutta 700098, India.

e-mail: anita@bose.res.in

Abstract. We investigate the full phase diagram of a column of grains near jamming, as a function of varying levels of frustration. Frustration is modelled by the effect of two opposing fields on a grain, due respectively to grains above and below it. The resulting four dynamical regimes (ballistic, logarithmic, activated and glassy) are characterised by means of the jamming time of zero-temperature dynamics, and of the statistics of attractors reached by the latter. Shape effects are most pronounced in the cases of strong and weak frustration, and essentially disappear around a mean-field point.

PACS. 64.60.My Metastable phases – 45.70.Cc Static sandpiles; granular compaction – 45.70.Vn Granular models of complex systems; traffic flow – 64.70.Q- Theory and modeling of the glass transition

1 Introduction

One of the reasons why heterogeneities are intrinsic to granular media is the absence of thermal motion; spatial and temporal behaviour has no reason to equilibrate, so that structures as well as time tracks which are far out of equilibrium can remain juxtaposed in the same system. Clearly, this leads to spatially and dynamically heterogeneous behaviour. It is, however, only recently that research efforts in this context have focused on heterogeneity (see [1] for a recent review). Examples of static spatial heterogeneity in granular systems include bridges [2,3,4] and force chains [5]. More generally, dynamical heterogeneities have attracted a lot of attention recently, both in granular matter (see [6]) and in other systems such as glasses or colloids (see [7]).

Spatiotemporal heterogeneity takes place when different parts of a system have diverse dynamical behaviour characteristic of their location. The first indications of such heterogeneity in a vibrated granular medium were found in the experiments of Reference [8], the findings of which indicated that both the average density, as well as density fluctuations, varied strongly throughout a shaken box of grains as a function of depth. Computer simulation and theoretical results [9] reproduced this behaviour, predicting additionally that the mean density was an increasing function of depth, and that density fluctuations were largest in the middle of the box for time windows relevant to experiment. These results additionally suggested that the phase behaviour within the box was very heterogeneous; ballistic behaviour was expected near the top, activated in the middle and glassy behaviour at its base.

The theoretical model [10,11,12,13] on the basis of which the latter predictions were made is as follows: grains in a column are able to orient themselves in one of two possible ways, corresponding to ‘ordered’ and ‘disordered’. When a grain is in its disordered orientation, space is wasted: a void of size ε is created, which characterises the shape of the grain. Rational and irrational values of ε correspond to regular and irregular grain shapes respectively. Despite the simplicity of this ‘aspect ratio’ formulation of shape effects, recent work [14] has shown that it may be used to characterise a rich variety of granular shapes.

The presence of gravity is included in the model by a depth-dependent local frequency, such that lower (more weight-bearing) grains move more slowly than the less burdened upper grains. In the jamming limit, voids are minimized; accordingly, the definition of a ground state in the model is one that locally minimizes the voids ratio [2]. However, since the orientation that minimizes voids with respect to grains above a given grain is not typically that which fulfils the same function for those below itself, this naturally generates *frustration*. In the model, this is represented by the effect of two oppositely directed fields whose relative strengths are modulated by a coupling constant g .

In earlier work [10,11,12,13], the focus was on the effect of shape; the behaviour of the model for typical rational and irrational values of the shape parameter ε was explored for $g = 0$ [11,12] and then in the $g \rightarrow 0$ limit [13]. Here we complete the analysis by looking at the effect of varying the coupling constant g . This is equivalent to vary-

ing the frustration, and as will be shown, has wide-ranging effects on the behaviour of the model.

The plan of the paper is as follows. The definition of the model is recalled in Section 2. Section 3 is devoted to the statics of the model, i.e., the number and the nature of its ground states. We then address the properties of zero-temperature dynamics. Section 4 contains an analysis of the dynamical phase diagram and of the behaviour of the jamming time in the various regimes, whereas the statistics of attractors is investigated in Section 5. In Section 6 we conclude with a brief discussion of our findings.

2 The model

In its most complete form, the model [13] consists of a finite column of N grains, labeled by their depth $n = 1, \dots, N$. Each grain has an orientation variable $\sigma_n = \pm 1$. Grain n is referred to as *up* or *ordered* when $\sigma_n = +1$ and *down* or *disordered* when $\sigma_n = -1$. Disordered orientations generate voids and waste space, whereas ordered ones do not. Implicit in this description is the effect of shape, which is most easily understood in terms of the rectangular grains of aspect ratio a considered in [10]. Grains aligned along their long edges (length 1) result in a fully packed column, whereas those perched on their short edges (length $a < 1$) leave voids of size $\varepsilon = 1 - a$. The horizontal orientation is thus ordered, and the vertical one disordered. Such a two-state model is clearly an approximation; we lump the effects of all possible void spaces created by disordered orientations of arbitrarily shaped grains into one disordered (vertical) orientation, and make a similar approximation for the ordered (horizontal) orientation.

The N binary variables $\{\sigma_n = \pm 1\}$ define the 2^N configurations of the system. We consider the following continuous-time stochastic dynamics which do not obey detailed balance. Grain orientations are updated with the Markovian rates

$$\begin{cases} w(\sigma_n = +1 \rightarrow \sigma_n = -1) = e^{-(\lambda_n + H_n)/\Gamma}, \\ w(\sigma_n = -1 \rightarrow \sigma_n = +1) = e^{-(\lambda_n - H_n)/\Gamma}, \end{cases} \quad (2.1)$$

where

- Γ is a dimensionless vibration intensity, referred to as temperature.
- λ_n is the activation energy of grain n , which we take to be proportional to its depth:

$$\lambda_n = \frac{n\Gamma}{\xi_{\text{dyn}}}. \quad (2.2)$$

The *dynamical length* ξ_{dyn} is the depth beyond which grains are frozen out by the sheer weight of grains above them. Thus, the frequency of response of a grain n falls off exponentially with its depth:

$$\phi_n = e^{-\lambda_n/\Gamma} = e^{-n/\xi_{\text{dyn}}}. \quad (2.3)$$

- H_n is the local ordering field felt by grain n , which is determined by all the other grains, both above and below n . The effect of the upper grains is assumed to be

uniform. The back-propagation from grains below a given grain cannot, of course, be similarly uniform. We assume for simplicity that upward constraints are exponentially damped, with a characteristic length ξ_{int} , the *interaction length*. We thus write

$$H_n = h_n + gj_n, \quad (2.4)$$

where the uniform effect h_n of grains above n ($m = 1, \dots, n-1$) and the non-uniform effect j_n of grains below n ($m = n+1, \dots, N$) are given by

$$h_n = \sum_{m=1}^{n-1} f(\sigma_m), \quad j_n = \sum_{m=n+1}^N f(\sigma_m) e^{-(m-n)/\xi_{\text{int}}}, \quad (2.5)$$

whereas g is a positive coupling constant.

Furthermore, both components h_n and j_n of the total local field H_n acting on grain n depend on every grain orientation $\sigma_m = \pm 1$ through the same function, the ‘shape factor’ $f(\sigma_m)$, where

$$f(\sigma) = \frac{\varepsilon - 1}{2} - \frac{\varepsilon + 1}{2} \sigma = \begin{cases} \varepsilon & \text{if } \sigma = -1, \\ -1 & \text{if } \sigma = +1. \end{cases} \quad (2.6)$$

The parameter ε can be thought of as the size of a typical void space for a grain of a particular shape, with rational and irrational values of ε corresponding to regular and irregular grain shapes respectively. There is an exact symmetry between models with ε and $1/\varepsilon$, so that the shape parameter can be restricted to $0 \leq \varepsilon \leq 1$.

Putting all of this together, we see that the contribution of an ordered grain to the local field is (negative) unity, while that of a disordered grain is a void space of magnitude ε ; the latter is clearly a function of granular shape, hence the name given to the shape factor $f(\sigma_m)$. The minus sign in the ordered case ensures that the contribution of an ordered grain to the excess void space H_n is *less* than that of a disordered grain, as it ought to be; more importantly, this says that a void space is destroyed every time a grain aligns in an ordered fashion relative to its neighbours.

The dynamics of the model involves the often conflicting contributions of the opposing local fields h_n and j_n . In turn, these comprise all the terms $f(\sigma_m)$ which take values ε or -1 according to (2.6), for all the other grains m in the column. As mentioned above, this represents a simple-minded way of incorporating frustration into the model.

In the following, we use the notation

$$x_{\text{int}} = e^{-1/\xi_{\text{int}}}. \quad (2.7)$$

We mention the following recursion relations:

$$h_n = h_{n-1} + f(\sigma_{n-1}), \quad j_n = x_{\text{int}} (f(\sigma_{n+1}) + j_{n+1}), \quad (2.8)$$

with $h_1 = j_N = 0$, which provide a fast algorithm to evaluate the local fields.

To sum up, the model parameters are the number of grains N , the shape parameter ε , the coupling constant g , and the interaction and dynamical lengths ξ_{int}

and ξ_{dyn} . Previous work has been devoted to investigations of zero-temperature static (number and structure of ground states) and dynamic (recovery of ground states as attractors) properties of the model in several special cases of interest: the directed model ($g = 0$) for $\xi_{\text{dyn}} = \infty$ [11], the directed model for general ξ_{dyn} [12], and the weak-coupling regime ($g \ll 1$) for $\varepsilon = 1$ [13].

In this work we aim at giving an overall picture of zero-temperature properties of the model all over its parameter space, with an emphasis on their dependence on the coupling constant g and on the lengths ξ_{int} and ξ_{dyn} . As some of the features of the model are different for rational and irrational values of the shape parameter ε , we shall use $\varepsilon = 1$ as our prototypical rational number, and the (small) golden mean

$$\varepsilon = \frac{1}{\Phi} = \frac{\sqrt{5}-1}{2} \approx 0.618033 \quad (2.9)$$

as our prototypical irrational number.

3 Statics: ground states

The rules (2.1) simplify as follows in the zero-temperature limit ($\Gamma \rightarrow 0$):

$$\frac{w(\sigma_n = -1 \rightarrow \sigma_n = +1)}{w(\sigma_n = +1 \rightarrow \sigma_n = -1)} = e^{2H_n/\Gamma} \rightarrow \begin{cases} \infty & \text{if } H_n > 0, \\ 0 & \text{if } H_n < 0. \end{cases} \quad (3.1)$$

It is therefore natural to define a *ground state* as a configuration where the orientation of every grain is aligned along its local field [10,11,12,13]:

$$\sigma_n = \text{sign } H_n = \begin{cases} +1 & \text{if } H_n > 0, \\ -1 & \text{if } H_n < 0. \end{cases} \quad (3.2)$$

We start with two special cases where the analysis of ground states is simpler.

3.1 Directed model ($g = 0$)

The ground states of the directed model have been investigated in [11,12]. In that case, the local field $H_n = h_n$ acting on grain n only depends on the grains above n . The expression (3.2) therefore boils down to the following recursion relation:

$$\begin{cases} h_n > 0 \implies \sigma_n = +1, & h_{n+1} = h_n - 1, \\ h_n < 0 \implies \sigma_n = -1, & h_{n+1} = h_n + \varepsilon, \end{cases} \quad (3.3)$$

with initial values $h_1 = 0$, and $\sigma_1 = +1$ for definiteness. In a ground state, all the local fields h_n lie in the range

$$-1 \leq h_n \leq \varepsilon. \quad (3.4)$$

The boundedness of the local fields implies that all the ground states have the same mean orientation $\langle \sigma \rangle$, such that $\langle f(\sigma) \rangle = 0$, hence

$$\langle \sigma \rangle = \frac{\varepsilon - 1}{\varepsilon + 1}, \quad (3.5)$$

up to fluctuations which become negligible for large systems.

The number and the nature of ground states depend on whether ε is rational or irrational.

If the shape parameter ε is irrational, the recursion formula (3.3) implies that all the local fields h_n are non-zero (except $h_1 = 0$). A *unique quasiperiodic ground state* is thus generated. Had we made the initial choice $\sigma_1 = -1$, we would have obtained the same configuration, up to a permutation of the two uppermost grains, so that the model has in all two ground states. For the golden mean (2.9), the ground-state grain configuration is given by a Fibonacci sequence:

$$\{\sigma_n\} = + - - + - - + - - + - - + - - + - - \dots \quad (3.6)$$

If the shape parameter ε is rational, i.e.,

$$\varepsilon = \frac{p}{q} \quad (3.7)$$

in irreducible form (p and q mutual primes), some of the local fields h_n generated by the recursion (3.3) vanish. The corresponding grain orientations σ_n remain unspecified. This orientational indeterminacy occurs at points of perfect packing, such that $n - 1$ is a multiple of the *period* $p + q$. The model therefore has *extensively degenerate ground states*. Every one of them is a random sequence of two well-defined patterns of length $p + q$, such that each pattern contains p up and q down grains. Defining the static (configurational) entropy per grain as

$$\Sigma = \frac{\ln \mathcal{N}_N}{N}, \quad (3.8)$$

where \mathcal{N}_N is the number of ground states of a system consisting of N grains, we have therefore

$$\Sigma = \frac{\ln 2}{p + q} \quad (3.9)$$

in the limit of a large system. The simplest of all rational values is $\varepsilon = 1$, i.e., $p = q = 1$. In this symmetric case, we have $f(\sigma) = -\sigma$, so that both orientations play symmetric rôles. The ground states are all the *dimerised* configurations, made of the patterns $+-$ and $-+$. The static entropy here assumes its maximal value $\Sigma = (\ln 2)/2$.

3.2 Mean-field point ($g = 1$, $\xi_{\text{int}} = \infty$)

This situation is the complete opposite of the previous one. Upper and lower grains have equal weights, so that both components h_n and j_n of the local field add up to give

$$H_n = \eta - f(\sigma_n), \quad (3.10)$$

where we have introduced the *mean field*

$$\eta = \sum_{m=1}^N f(\sigma_m) = \varepsilon N^- - N^+ = \varepsilon N - (\varepsilon + 1)N^+, \quad (3.11)$$

with N^+ and $N^- = N - N^+$ being respectively the numbers of up grains and of down grains in the configuration. The above expression shows that η is a *global* measure of excess void space [2] in the system. This globality results from the exact cancellation of fluctuations in the local void space corresponding to the competing fields h_n and j_n ; mean-field behaviour thus replaces the local fluctuations of the general case. In this limit, the model resembles the one studied in [10], one of the earliest building blocks of the present model. We shall comment on further analogies between both models in due course.

The condition (3.2) thus reads

$$\sigma_n = \text{sign}(\eta - f(\sigma_n)). \quad (3.12)$$

It is fulfilled for all grains n as soon as the mean field lies in the range $-1 \leq \eta \leq \varepsilon$. These inequalities amount to saying that N^+ takes a well-defined ground-state value:

$$N_{\text{gs}}^+ = \text{Int} \left(\frac{\varepsilon N + 1}{\varepsilon + 1} \right), \quad (3.13)$$

where $\text{Int}(x)$, the integer part of x , is the largest integer less than or equal to x . The result (3.5) is recovered in the limit of a large system.

At the mean-field point, the ground states are all the configurations consisting of N_{gs}^+ up grains and $N_{\text{gs}}^- = N - N_{\text{gs}}^+$ down grains. The number of ground states is therefore

$$\mathcal{N}_N = \binom{N}{N_{\text{gs}}^+}, \quad (3.14)$$

so that the static entropy per grain reads

$$\Sigma = \ln(\varepsilon + 1) - \frac{\varepsilon}{\varepsilon + 1} \ln \varepsilon. \quad (3.15)$$

This result will be illustrated in Figure 2.

3.3 General case

We now turn to the general case. The behaviour of the model turns out to be dictated mainly by the coupling constant g , whereas the effect of the other parameters ε or ξ_{int} is less pronounced. The difference between rational and irrational values of ε , which is the most salient feature of the directed model, manifests itself most in the weak-coupling and strong-coupling regimes ($g \ll 1$ and $g \gg 1$). The overall picture, already sketched in [13], is the following.

If the shape parameter ε is irrational, the static entropy rises continuously from zero and behaves linearly at weak coupling:

$$\Sigma \approx Ag \quad (g \ll 1), \quad (3.16)$$

where the amplitude A depends on ε and ξ_{int} . The meaning of this result [13] is that generic ground states consist of quasiperiodic patches whose typical length diverges as $L(g) \sim 1/g$ at weak coupling. The entropy then smoothly

increases as a function of g , reaches a maximum around the mean-field coupling $g = 1$, and smoothly falls off to zero for $g \gg 1$.

If the shape parameter ε is rational, the static entropy stays equal to its value (3.9) over a whole range $0 \leq g \leq g_s$, where g_s (with ‘s’ for static) is the *static threshold*. As already underlined in [13], evaluating g_s is a non-trivial task in general. The simplest situation is for $\varepsilon = 1$ and an even number of grains ($N = 2K$). The ground states in the directed case ($g = 0$), and by continuity at weak enough coupling, are the 2^K dimerised ones. It can then be argued, thinking along the lines of [13], that the first non-dimerised ground states which appear upon increasing g are $++--(-+)^{K-2}$ and $--++(+)^{K-2}$, and that the relevant grain orientation for their stability is the second one (σ_2). Consider the first configuration for concreteness. We have $h_2 = -1$ and $j_2 = x_{\text{int}} + x_{\text{int}}^2 + x_{\text{int}}^3 - x_{\text{int}}^4 + \dots + x_{\text{int}}^{2K-3} - x_{\text{int}}^{2K-2}$. The above configurations become ground states for $H_2 = h_2 + gj_2 > 0$, i.e., $g > g_s = |h_2|/j_2$. We thus obtain

$$g_s = \frac{1 + x_{\text{int}}}{x_{\text{int}}(1 + 2x_{\text{int}} + 2x_{\text{int}}^2 - x_{\text{int}}^{N-2})}, \quad (3.17)$$

and for an infinitely large system

$$g_s = \frac{1 + x_{\text{int}}}{x_{\text{int}}(1 + 2x_{\text{int}} + 2x_{\text{int}}^2)}. \quad (3.18)$$

Figure 1 shows a plot of the static entropy Σ against g for a column of $N = 20$ grains with $\xi_{\text{int}} = 10$, for both shape parameters $\varepsilon = 1$ and $\varepsilon = 1/\Phi$. The exact number of ground states is obtained by means of a full enumeration of the 2^{20} configurations. The distinction between rational and irrational ε is visible at weak coupling. For $\varepsilon = 1$ (our prototype of a rational), Σ remains equal to $\Sigma = (\ln 2)/2 \approx 0.346573$ in the whole range $0 \leq g \leq g_s$, where the static threshold reads $g_s \approx 0.491651$, including the finite-size effect of (3.17). For $\varepsilon = 1/\Phi$ (our prototype of an irrational), Σ rises continuously from the minimal value $(\ln 2)/N$, i.e., essentially zero, up to a finite-size effect due to the existence of two ground states.

Besides this, the static entropy has a weak dependence on the shape parameter ε . Both for rational and irrational ε , the entropy has a smooth maximum around the mean-field point ($g = 1$), and it falls off smoothly at large g . The increase in the static entropy as the coupling g increases from 0 to 1 reflects the progressive decrease of the amount of order in the ground states. For an irrational ε , this corresponds to a shortening of the coherence length $L(g)$ with increasing g . Finally, the weak dependence of the entropy on ε near its maximum, i.e., near the mean-field point, is an early indication that shape dependence is increasingly lost as the model become more and more mean-field-like.

A digression on the effects of shape

As mentioned above, increasing the value of g corresponds to increasing the frustration. As soon as the coupling constant g takes appreciable values, the evolution of ordering

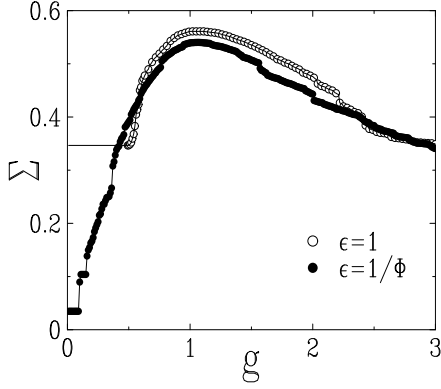


Fig. 1. Plot of the static entropy Σ against the coupling constant g for a column of $N = 20$ grains with $\xi_{\text{int}} = 10$ for both shape parameters $\varepsilon = 1$ and $\varepsilon = 1/\Phi$. For $\varepsilon = 1$, the first symbol is at the threshold $g_s \approx 0.491651$ (see (3.17)).

due to compaction no longer proceeds in a top-down fashion, as it did in the directed ($g = 0$) model [10,11,12]. We outline here what we might expect for the dynamical behaviour in the case of general g , before making specific calculations.

Looking at zero-temperature dynamics allows us to get a flavour of the ordering behaviour. Do grains retrieve their ground states in the limit of zero perturbation, and if so, how? In the case of $g = 0$, the effect of the shape parameter ε is maximal on the zero-temperature dynamics [10,11,12]: irregularly shaped grains with irrational ε order ballistically fast into their unique quasiperiodic ground state, while regularly shaped grains never retrieve any of their many ground states, manifesting density fluctuations instead, due to the presence of many sites where $h_n = 0$ [11,12]. Similar behaviour has been observed in experiments [8] on vibrated granular beds, from which we can infer that the effects of frustration, if any, are negligible compared to the intensity of vibration in the experiment under consideration.

For a low but non-zero coupling g , the ‘reverse’ field j_n induces some frustration as it begins to impose its own order in an upward direction, competing with the downward ordering due to h_n . In the case of irrational ε , one might imagine that the effect of the reverse ordering would break up the unique quasiperiodic ground state corresponding to $g = 0$; while in the case of rational ε , even the tiniest amount of frustration ensures that points of zero field are not constantly generated and re-generated, and hence that the density fluctuations of the $g = 0$ case disappear. The only possible logical culmination of ordering from *both* the top and the bottom of the column might be to ‘fix’ the points of zero field; in the case of $\varepsilon = 1$ this corresponds to a dimerisation of the ground states. These were indeed the findings of earlier work [13].

Increasing frustration beyond these values might in a general sense lead to the breakdown of even this level of order. While the details would depend on parameters like ξ_{int} and ξ_{dyn} , we mention a few likely outcomes. For both weak ($g \ll 1$) and extremely strong ($g \gg 1$) cou-

plings, we might expect the prevalence of very similar order, although propagating in opposite directions (top-down in the first, and upwards in the second case). At the mean-field point ($g = 1$, $\xi_{\text{int}} = \xi_{\text{dyn}} = \infty$), where the fluctuations in both ordering fields cancel each other, the system of grains is totally uncorrelated, leading to a situation similar to that explored in [10]. The gradual replacement of the ordering by individual grains by the ordering of granular clusters might be expected to occur for g in the vicinity of the mean-field point ($g = 1$); shape effects are therefore expected to be minimal here.

The results of the next two sections will bear out some of these speculations.

4 Dynamics: jamming time

The rules for zero-temperature dynamics are defined as follows [11,12,13]. The uppermost grain is kept fixed to

$$\sigma_1 = +1. \quad (4.1)$$

The other grains ($n = 2, \dots, N$) are selected at a rate given by (2.3). Once a grain is selected, its orientation σ_n is aligned along the local field H_n according to the deterministic rule

$$\sigma_n \rightarrow \text{sign } H_n, \quad (4.2)$$

provided the local field H_n does not vanish. The choice of boundary condition (4.1) is motivated by the fact that the strongest component in the local field H_n is typically the long-ranged component h_n which propagates via gravity. As a consequence, interactions propagate downwards in general, so that it is natural to impose a boundary condition at the top of the column. We assume that the column is prepared in a random state, where each grain is oriented at random ($\sigma_n = \pm 1$ with equal probabilities for all $n \geq 2$).

The above rule is well-defined for a non-zero coupling constant g , because the local fields H_n do not vanish in general. The zero-temperature dynamics thus defined leads to *metastability*. A finite column of N grains is eventually driven to an absorbing configuration or *attractor*, in a finite *jamming time* T . This attractor is necessarily one of the ground states described earlier, i.e., a configuration where every orientation σ_n is aligned with H_n . Let us emphasize that imposing a restrictive boundary condition, i.e., fixing one of the spins (see (4.1)), is necessary to have metastability in the above sense. Without such restriction, zero-temperature dynamics would drive a finite system to a fluctuating steady state.

In the present context, ‘metastable state’, ‘attractor’ and ‘ground state’ are therefore essentially synonymous. Arbitrary initial conditions can lead to any one of the ground states being reached. They are however *fragile*, in the sense that a slightly different initial condition or stochastic history leads to another attractor being reached in general. This fragility [15] of metastable states is one of the characteristics of granular media [16].

Along the lines of [13], we will focus on two aspects of zero-temperature dynamics, namely the statistics of the

jamming time (in this Section) and that of the attractors (in Section 5). The jamming time is doubly random, as it depends both on the initial configuration of the system and on its whole stochastic history. Just as for statics, we begin with a few special cases.

4.1 Directed model ($g = 0$)

The dynamical behaviour of the directed column has been studied at length [11,12]. It depends qualitatively on whether ε is rational or irrational.

If the shape parameter ε is irrational, its unique quasiperiodic ground state is reached by ballistic coarsening. An upper layer of the column is ordered, whose thickness grows linearly with time (the ballistic phase will be described more thoroughly in Section 4.3). The dependence of the corresponding velocity V on ε has been investigated in [12].

If the shape parameter $\varepsilon = p/q$ is rational, the local field h_n may vanish whenever $n - 1$ is a multiple of the period $p + q$. It is therefore natural to complete the dynamical rule (4.2) as [11,12]:

$$\sigma_n \rightarrow \begin{cases} + & \text{if } h_n > 0, \\ \pm & \text{with prob. } 1/2 \text{ if } h_n = 0, \\ - & \text{if } h_n < 0. \end{cases} \quad (4.3)$$

These dynamical rules do not drive the system to any of its ground states. There are always grains whose local fields h_n vanish. The column reaches a non-trivial fluctuating steady state, investigated in [12], which exhibits anomalous roughening: the fluctuations in the local field grow with a power law, as $\langle h_n^2 \rangle \sim n^{2/3}$.

4.2 Mean-field point ($g = 1, \xi_{\text{int}} = \infty$)

It has been shown in Section 3.2 that the statics of the model is of a mean-field type when $g = 1$ and $\xi_{\text{int}} = \infty$.

This property extends to the dynamics in the $\xi_{\text{dyn}} = \infty$ limit, where activation energies are negligible, so that grains are sampled uniformly and the effect of gravity is lost. In this limit, the dynamical rule (4.2) indeed becomes

$$\sigma_n \rightarrow \text{sign}(\eta - f(\sigma_n)), \quad (4.4)$$

where η is the mean field introduced in (3.11). Thus every grain orientation σ_n is updated to $+1$ (resp. -1), with unit rate, irrespective of its position n , as long as $\eta > \varepsilon$ (resp. $\eta < -1$). This rule can be recast as the following effective dynamics for the number N^+ of up spins:

$$\begin{cases} N^+ < N_{\text{gs}}^+ \implies N^+ \rightarrow N^+ + 1 & \text{with rate } N - N^+, \\ N^+ > N_{\text{gs}}^+ \implies N^+ \rightarrow N^+ - 1 & \text{with rate } N^+. \end{cases} \quad (4.5)$$

The dynamics stop as soon as N^+ reaches the value N_{gs}^+ (see (3.13)), i.e., when the system reaches a ground state.

Mean-field zero-temperature dynamics are fast, in the strong sense that the jamming time is microscopic. More

precisely, consider $\varepsilon < 1$ for definiteness, so that $N_{\text{gs}}^+ < N/2$. For a random initial configuration, characterised by $N^+ \approx N/2$, the mean jamming time can be shown to read (see e.g. [17])

$$\langle T \rangle \approx \sum_{N^+=N_{\text{gs}}^+}^{N/2} \frac{1}{N^+} \approx \ln \frac{\varepsilon + 1}{2\varepsilon} \quad (4.6)$$

for a large system. The jamming time is indeed found to be microscopic. This makes good physical sense, since the system is fully uncorrelated, and all the grains are simultaneously mobile.

Furthermore, as N^+ is the only non-trivial dynamical variable, it is clear that all the ground states are reached with uniform probability. In other words, anticipating the discussion of Section 5, the mean-field dynamics of our column model ($g = 1, \xi_{\text{int}} = \xi_{\text{dyn}} = \infty$) is one of the rare instances where Edwards' flatness hypothesis [18] can be shown to be exactly valid. A similar result has been established in the context of the ageing dynamics of mean-field spin-glass models [19].

Rôle of a finite ξ_{dyn}

We now study the model at its static mean-field point, but with generic dynamics defined by a finite value of the dynamical length ξ_{dyn} . This situation is of interest because it is both simple (the updating rule is still given by (4.4)), and non-trivial (grains are not selected uniformly anymore). Grain n is indeed updated at a rate given by (2.3), so that upper grains are more mobile than lower ones. This case is physically similar to that of a column of non-interacting grains in the presence of gravity [10].

Consider again $\varepsilon < 1$ for concreteness. For a random initial configuration, the typical number of grains to be flipped from $+$ to $-$ reads

$$N_{\text{f}} \approx \frac{N}{2} - N_{\text{gs}}^+ \approx \frac{1 - \varepsilon}{2(1 + \varepsilon)} N. \quad (4.7)$$

It is worth considering first the slow regime ($N \gg \xi_{\text{dyn}}$). In this situation, the grains to be flipped are essentially the N_{f} uppermost $+$ grains, which occupy an upper layer of depth $2N_{\text{f}}$ in a random initial state. As a consequence, the jamming time scales as $T \sim \exp(2N_{\text{f}}/\xi_{\text{dyn}})$, i.e.,

$$T \sim \exp\left(\frac{1 - \varepsilon}{1 + \varepsilon} \frac{N}{\xi_{\text{dyn}}}\right). \quad (4.8)$$

The jamming time therefore grows exponentially with N . The prefactor is proportional to that entering the asymptotic orientation (3.5). As a consequence, (4.8) does not apply to the symmetric situation ($\varepsilon = 1$), where the jamming time is not exponentially large in N in this regime. Large jamming times testify that the retrieval of ground states is not easy; they are likely to correspond to lower dynamical entropies. The ε -dependent prefactor suggests

that shape effects would be strongly related to the absence of Edwards flatness, as will be verified below. Furthermore, the typical orientation profile of an attractor takes the form of a discontinuous step:

$$\langle \sigma_n \rangle \approx \begin{cases} -1 & (n < 2N_f), \\ 0 & (2N_f < n < N). \end{cases} \quad (4.9)$$

We define the zero-temperature dynamical entropy per grain as

$$S = -\frac{1}{N} \sum_{\mathcal{C}} Q(\mathcal{C}) \ln Q(\mathcal{C}), \quad (4.10)$$

where the sum runs over the attractors \mathcal{C} , and where $Q(\mathcal{C})$ is the probability that the dynamics drive the system into attractor number \mathcal{C} , starting from a random initial condition. The above picture of jamming in the slow regime leads to the estimate $NS \approx (N - 2N_f) \ln 2$, as the difference $N - 2N_f$ is an estimate of the number of the lower grains which do not move during the history of the column. The dynamical entropy therefore reads

$$S = \frac{2\varepsilon}{1 + \varepsilon} \ln 2. \quad (4.11)$$

This quantity is smaller than the static entropy Σ , given by (3.15). Both entropies indeed only coincide at the extremal values $\varepsilon = 0$ (where $\Sigma = S = 0$) and $\varepsilon = 1$ (where $\Sigma = S = \ln 2$). The entropy difference is maximal for $\varepsilon = 1/4$, where it equals $\Sigma - S = \ln(5/4) \approx 0.223143$. Figure 2 presents a comparison between both entropies. This slow mean-field regime is one of the rare cases where the violation of Edwards' flatness can be turned into a quantitative estimate. Another zero-temperature example is provided by kinetically constrained one-dimensional spin models [20].

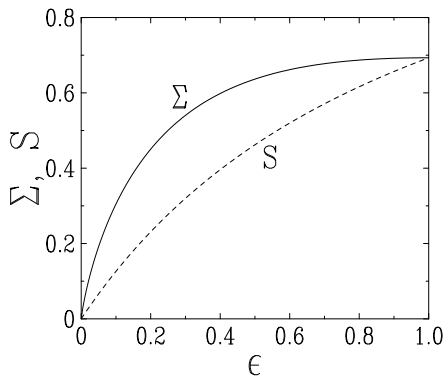


Fig. 2. Comparison between static and dynamical zero-temperature entropies against the shape parameter ε in the range $0 \leq \varepsilon \leq 1$, in the slow regime of the mean-field model ($g = 1$, $\xi_{\text{int}} = \infty$, $N \gg \xi_{\text{dyn}}$). Upper full curve: static entropy Σ (see (3.15)). Lower dashed curve: dynamical entropy S (see (4.11)).

For generic values of the ratio N/ξ_{dyn} , the attractor statistics vary continuously between the uniform case of

mean-field dynamics (for $N \ll \xi_{\text{dyn}}$) and the non-uniform case of the slow regime, described above (for $N \gg \xi_{\text{dyn}}$). This continuous dependence is best visualised by the orientation profile $\langle \sigma_n \rangle$ of the attractors. Figure 3 shows numerical data for the orientation profile with $\varepsilon = 1/\Phi$ and $N = 200$. Each dataset is obtained by averaging over 10^6 different stochastic histories with different initial configurations. The data demonstrate a continuous crossover between a uniform profile at the mean value (3.5), i.e., $\langle \sigma \rangle = -1/\Phi^3 \approx -0.236067$ (for $N \ll \xi_{\text{dyn}}$) and the discontinuous step profile (4.9) of the slow regime (for $N \gg \xi_{\text{dyn}}$).

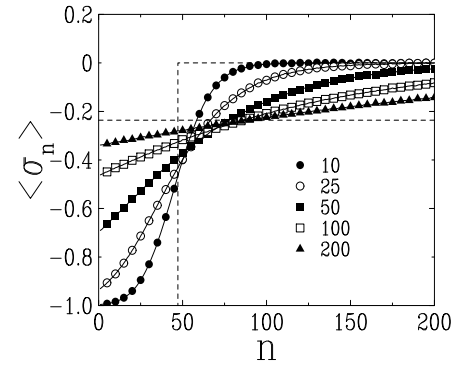


Fig. 3. Plot of the orientation profile $\langle \sigma_n \rangle$ of the attractors against depth n at the static mean-field point ($g = 1$, $\xi_{\text{int}} = \infty$) for $\varepsilon = 1/\Phi$ and $N = 200$. Symbols: data for several values of ξ_{dyn} . Dashed lines: limiting uniform and step profiles, respectively corresponding to $N \ll \xi_{\text{dyn}}$ and $N \gg \xi_{\text{dyn}}$.

4.3 Full dynamical phase diagram

We now turn to the zero-temperature dynamics of our model for generic parameter values. We expect that the phase diagram of the model can be roughly divided into three regions:

- (a) the weak-coupling regime ($g \ll 1$), already explored in earlier work for $\varepsilon = 1$ [13]; a strong uniform field h_n is the dominant effect, leading to a correspondingly strong dependence on the shape parameter ε ,
- (b) the neighbourhood of the mean-field point ($g = 1$), where ordering proceeds with fewer local constraints, so that shape dependence is increasingly lost,
- (c) the strong-coupling end ($g \gg 1$), where a strong frustrating field j_n is the dominant effect; this might be expected to lead to the return of a strong dependence on the shape parameter ε .

For the time being, we restrict our study to the case where $\xi_{\text{dyn}} = \infty$, so that grains are sampled uniformly by the dynamics. The dynamical properties of the model are mainly dictated by the coupling constant g and the interaction length ξ_{int} , with a less pronounced dependence on the shape parameter ε , except in the weak-coupling regime. The main features of the model are summarised in the dynamical phase diagram shown in Figure 4. This picture will be made more precise in the following.

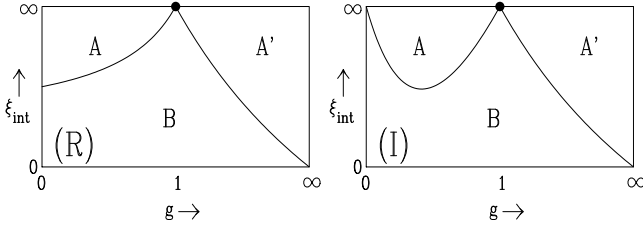


Fig. 4. Sketch of the phase diagram of the model in the g - ξ_{int} plane for a rational ((R), left) and irrational ((I), right) shape parameter ε . Symbol: mean-field point. Curves: critical lines $\xi_{\text{int}} = \xi_{\text{int},c}(g; \varepsilon)$. B: ballistic phase. A: weak-coupling activated phase. A': strong-coupling activated phase.

At this point, it is worth emphasising that the dynamical phase diagram of the model depends on the precise definition of zero-temperature dynamics, including the boundary condition (4.1). In particular, had we chosen to fix the bottommost spin (σ_N) instead of the uppermost one (σ_1), we would have obtained somewhat different phase boundaries; this would be true especially for large g , with a finite limiting $\xi_{\text{int},c}$ along the $g = \infty$ axis mirroring that which exists currently for $g = 0$. We will return to this point in Section 6.

The scenario observed for generic values of g qualitatively follows that of the weak-coupling ($g \ll 1$) regime for $\varepsilon = 1$, investigated in [13]. The model is in a ballistic phase if the interaction length is small ($\xi_{\text{int}} < \xi_{\text{int},c}$), and in an activated phase if the interaction length is large ($\xi_{\text{int}} > \xi_{\text{int},c}$). The critical value $\xi_{\text{int},c}$ of the interaction length ξ_{int} depends strongly on g and weakly on ε . Let us start by reviewing the main characteristics of both phases and of the crossover between them, which have been analyzed in [13].

• *Ballistic phase* ($\xi_{\text{int}} < \xi_{\text{int},c}$). In this phase, zero-temperature dynamics propagate order into the system from the top down [11,12,13]. More precisely, if we define the thickness $L(t)$ of the upper ordered layer of the column as the depth of the uppermost grain which is *not* aligned with its local field, the ballistic phase is characterised by a linear growth of the mean thickness:

$$\langle L(t) \rangle \approx Vt, \quad (4.12)$$

where V is the ballistic velocity. Fluctuations around this mean behaviour are due to diffusion. As a consequence, for a finite system of N grains, the jamming time grows linearly with N :

$$\langle T \rangle \approx \frac{N}{V}, \quad (4.13)$$

up to relatively negligible fluctuations, so that the reduced variance of the jamming time,

$$K_T = \frac{\text{var } T}{\langle T \rangle^2} = \frac{\langle T^2 \rangle}{\langle T \rangle^2} - 1, \quad (4.14)$$

is of order $1/N$.

• *Activated phase* ($\xi_{\text{int}} > \xi_{\text{int},c}$). In this phase, zero-temperature dynamics do not proceed in any ordered way. The

system explores its configuration space more or less uniformly, until it meets one of its ground states by chance. This picture is that of an activated phenomenon. An exponential growth of the mean jamming time with the column size results:

$$\langle T \rangle \sim e^{aN}, \quad (4.15)$$

at least for very large N , where a is the effective reduced activation energy per grain. In other words, the system has to cross an extensive entropic barrier, whose height grows asymptotically as aN , in order to reach a ground state. This also suggests an exponential distribution of jamming times, so that the reduced variance asymptotes to $K_T = 1$.

• *Diffusive crossover* ($\xi_{\text{int}} \approx \xi_{\text{int},c}$). The crossover between ballistic and activated behaviour has been shown [13] to be described by a simple effective model. The thickness $L(t)$ of the ordered layer was treated as a collective coordinate, and its dynamics modelled by biased Brownian motion (see Appendix B of [13]). In the ballistic regime, the downward propagation of the layer is helped by the dominant effect of the field h_n , while in the activated regime, it is hindered by the dominant effect of the field j_n . The crossover thus corresponds to the point $\xi_{\text{int}} = \xi_{\text{int},c}$ where the effects of the two fields are neutralised. The behaviour right at the crossover is dictated by the presence of a diffusive critical point. Observables obey finite-size scaling laws involving the scaling variable $z = \alpha X + \beta$, with $X = N(\xi_{\text{int}} - \xi_{\text{int},c})$, whereas α and β are non-universal numbers. For instance, the mean jamming time $\langle T \rangle$ and its reduced variance K_T obey

$$\langle T \rangle \approx \frac{N^2}{2D} F(z), \quad K_T \approx G(z), \quad (4.16)$$

where D is an effective diffusion constant, whereas F and G are known universal scaling functions. The reduced variance of the jamming time takes the non-trivial universal value $K_T = G(0) = 2/3$ right at the critical point, i.e., for $z = 0$ or $\xi_{\text{int}} \approx \xi_{\text{int},c} - \beta/(\alpha N)$. In practice the $1/N$ correction is negligible for $N/\xi_{\text{int},c} > 10$. Measuring K_T thus provides an efficient way of exploring the dynamical phase diagram.

We now turn to the presentation and discussion of actual numerical data. Figure 5 shows a plot of the ballistic velocity V against the coupling constant g , for both shape parameters $\varepsilon = 1$ and $\varepsilon = 1/\Phi$, and for two values of the interaction length ($\xi_{\text{int}} = 3$ and 5) deep in the ballistic phase, i.e., much smaller than $\xi_{\text{int},c}$. For the irrational shape parameter $\varepsilon = 1/\Phi$, the velocity V departs continuously from its value in the directed model ($g = 0$), i.e., $V \approx 2.58$ [12]. It increases steadily and reaches its maximal value at or near the mean-field coupling ($g = 1$). If the shape parameter ε is rational, the velocity assumes a constant value over a whole range $0 \leq g \leq g_d$, where g_d (with ‘d’ for dynamical) is the *dynamical threshold*. Along the lines of [13], the latter can be shown to read

$$g_d = \frac{1 - x_{\text{int}}}{x_{\text{int}} \max(p, q)} = \frac{e^{1/\xi_{\text{int}}} - 1}{\max(p, q)} \quad (4.17)$$

for an arbitrary rational value $\varepsilon = p/q$ of the shape parameter. For $\varepsilon = 1$, this result reads

$$g_d = \frac{1 - x_{\text{int}}}{x_{\text{int}}} = e^{1/\xi_{\text{int}}} - 1. \quad (4.18)$$

This dynamical threshold is always smaller than its static counterpart (see (3.18)), as it should be. Both thresholds will be shown in Figure 8.

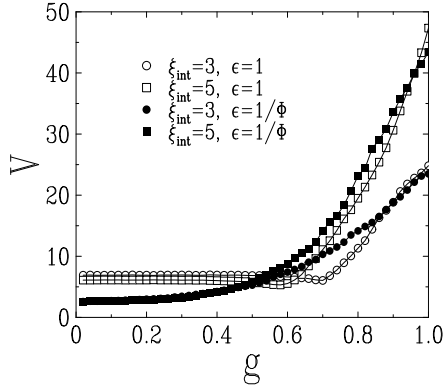


Fig. 5. Plot of the ballistic velocity V against the coupling constant g for several values of the parameters ξ_{int} and ε .

The *increase* of V with g to a maximum near the mean-field point, observed for both irrational and rational ε , seems apparently paradoxical, as increasing g after all increases the effects of frustration. The dynamics at the mean-field static point ($g = 1$) are however expected to be rather fast, irrespective of shape, so that the velocity can be expected to be both large and independent of ε near the mean-field point. We will return to this paradox later, when we investigate the scaling properties of the jamming time near the mean-field point.

Right at the mean-field coupling ($g = 1$), the ballistic velocity V is observed to depend strongly on ξ_{int} and weakly on ε , along the lines of the above discussion. It diverges faster than linearly at large ξ_{int} . In order to investigate this divergence, we present in Figure 6 a plot of the ratio V/ξ_{int} against $\xi_{\text{int}}^{1/2}$, for both shape parameters $\varepsilon = 1$ and $\varepsilon = 1/\Phi$. The largest velocities reached are $V \approx 1000$ for $\xi_{\text{int}} = 50$; velocities larger than this are hard to measure accurately. The observed linear behaviour of both datasets with equal slopes suggest the scaling behaviour

$$V(g = 1) \approx A \xi_{\text{int}}^{3/2}, \quad (4.19)$$

the prefactor $A \approx 2.2$ being seemingly independent of shape parameter. The exponent $3/2$ of the growth of the velocity, as mean-field dynamics are approached, can be justified heuristically as follows. First of all, the dynamics are expected to proceed by ordering not individual grains, but entire correlated clusters of typical length ξ_{int} . This already brings in a factor of ξ_{int} . Furthermore, if we consider one such piece after a microscopic time but before ordering, we see that typical fluctuations of the mean orientation around its ground-state value (3.13) are expected

to fall off as $\xi_{\text{int}}^{-1/2}$ (because of the law of large numbers). The formula (4.6) shows that the corresponding times also fall off as $\xi_{\text{int}}^{-1/2}$. This brings in an extra factor of $\xi_{\text{int}}^{1/2}$ to the velocity, providing a plausible mechanism for the exponent $3/2$ in (4.19).

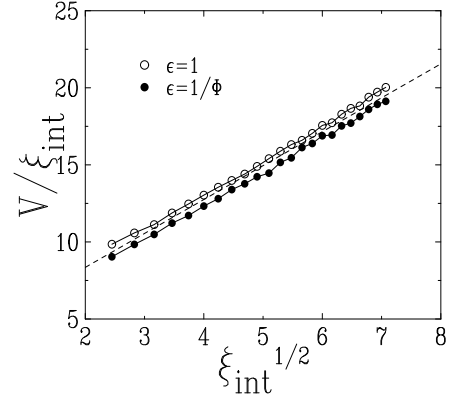


Fig. 6. Plot of the ballistic velocity V at the mean-field coupling ($g = 1$), divided by the interaction length ξ_{int} , against $\xi_{\text{int}}^{1/2}$, for both shape parameters $\varepsilon = 1$ and $\varepsilon = 1/\Phi$. The dashed line has slope 2.2.

We now present quantitative data for the phase diagram sketched in Figure 4. The position of the critical line $\xi_{\text{int},c}$ has been obtained by means of the criterion $K_T = 2/3$ for large enough systems, as explained in the paragraph below (4.16). Figure 7 shows plots of $\xi_{\text{int},c}$ against the coupling constant for both shape parameters $\varepsilon = 1$ and $\varepsilon = 1/\Phi$. In practice, values of $\xi_{\text{int},c}$ larger than 100 or 200 become very hard to measure with sufficient accuracy.

The critical value $\xi_{\text{int},c}$ is observed to diverge as $g \rightarrow 1$ from both sides, consistent with the result that mean-field dynamics are fast. The fits shown on Figure 7 as dashed lines suggest a quadratic divergence of the form

$$\xi_{\text{int},c} \approx \frac{B_1}{(g - 1)^2} \quad (4.20)$$

as mean-field coupling is approached from both sides. The amplitude is estimated to be $B_1 \approx 11 \pm 3$, irrespective of ε , albeit with a relatively large uncertainty. The above formula will be corroborated below by the finite-size scaling law (4.23).

The behaviour of $\xi_{\text{int},c}$ at weak coupling depends on whether ε is rational or not. For the rational shape parameter $\varepsilon = 1$, the non-trivial value $\xi_{\text{int},c} \approx 28.4$ at $g = 0$ [13] is recovered. For the irrational shape parameter $\varepsilon = 1/\Phi$, $\xi_{\text{int},c}$ is observed to diverge as $g \rightarrow 0$. The fit shown as a dashed line suggests a linear divergence of the form

$$\xi_{\text{int},c} \approx \frac{B_0}{g}, \quad (4.21)$$

with amplitude $B_0 \approx 0.8$. The above divergence can be explained in terms of the statics of the model. The quasiperiodic ground state obtained for irregular grains at

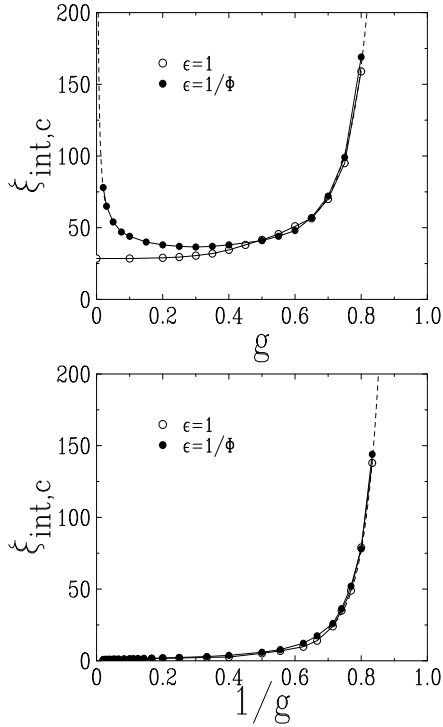


Fig. 7. Plot of the critical lines for both shape parameters $\varepsilon = 1$ and $\varepsilon = 1/\Phi$. Top: $\xi_{\text{int},c}$ separating phases A and B against g for $g < 1$. Bottom: $\xi_{\text{int},c}$ separating phases A' and B against $1/g$ for $g > 1$. Dashed lines: fits incorporating the divergence laws (4.20) with $B_1 = 11$ and (4.21) with $B_0 = 0.83$.

$g = 0$ splits into patches of typical length $L(g) \sim 1/g$ at small but non-zero coupling. As each of these quasiperiodic patches is retrieved coherently, it is natural to expect that the critical interaction length $\xi_{\text{int},c}$ should diverge in proportion to the static length $L(g)$ at weak coupling.

Since the critical interaction length $\xi_{\text{int},c}(g)$ diverges both as $g \rightarrow 0$ and $g \rightarrow 1$ for an irrational shape parameter, it must exhibit a minimum somewhere in the range $0 < g < 1$. For $\varepsilon = 1/\Phi$, this minimal value $\xi_{\text{int},c} \approx 36$, reached for $g \approx 0.3$, is in the same ballpark as the weak-coupling value $\xi_{\text{int},c} \approx 28.4$ for $\varepsilon = 1$. Soon after this minimum is attained, the values of $\xi_{\text{int},c}$ for $\varepsilon = 1$ and $\varepsilon = 1/\Phi$ begin to be nearly identical. One can therefore view the minimum in $\xi_{\text{int},c}$ as a crossover between a phase where the dynamics of individual grains (strong shape dependence) governs the retrieval of weak-coupling-like ground states, and another where the dynamics of clusters (little shape dependence) governs the retrieval of mean-field-like ground states. This viewpoint makes it clear why the most pronounced effects of shape occur before the crossover.

In the case of the rational shape parameter $\varepsilon = 1$, Figure 8 shows a comparison between the critical line in the g - ξ_{int} plane and the static and dynamical thresholds g_s and g_d , respectively given by (3.18) and (4.18). We recall that the dynamics is fully independent of g below the dynamical threshold ($0 < g < g_d$), whereas the attractors are exactly the dimerised configurations below the (larger) static threshold ($0 < g < g_s$). It turns out that

neither threshold has any effect on the fast (ballistic) or slow (activated) nature of the dynamics.

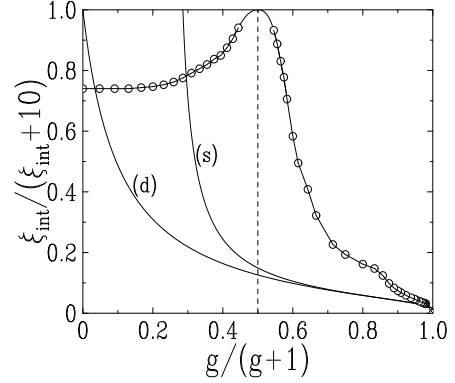


Fig. 8. Plot of notable lines in the g - ξ_{int} plane for $\varepsilon = 1$, providing a quantitative version of the left panel of Figure 4. Coordinates have been chosen for the sake of clarity. Left full line (d): dynamical threshold (4.18). Right full line (s): static threshold (3.18). Dashed line: mean-field coupling ($g = 1$). Line with symbols: critical line.

The three lines shown in Figure 8 seem to become close to each other in the lower right corner of the plot, i.e., at strong coupling, suggesting that one should look more closely at this regime. For large values of g , the dominant effect is that of the j_n field which propagates interactions upwards along the column. As a consequence, with our choice of fixing the uppermost spin (see (4.1)), the system will find it more and more difficult to order. This explains in qualitative terms why the critical line $\xi_{\text{int},c}$ falls off to zero at large g . The data shown in Figure 9 suggest an inverse logarithmic law for $\xi_{\text{int},c}$, of the form

$$\xi_{\text{int},c} \approx \frac{B_\infty}{\ln g}. \quad (4.22)$$

For the irrational shape parameter $\varepsilon = 1/\Phi$, the data show a smooth linear growth with slope $1/B_\infty \approx 0.275$, i.e., $B_\infty \approx 3.6$. For the rational shape parameter ε , the data are observed at first to follow those for $\varepsilon = 1/\Phi$, and then to cross over rather abruptly to a steeper regime of growth. The data seem to become asymptotically parallel to the static and dynamical thresholds g_s and g_d . If this observation holds quantitatively, we obtain the asymptotic slope $B_\infty = 1$ for $\varepsilon = 1$.

Vicinity of the mean-field point

We now turn to the study of the apparently paradoxical dependence of the jamming time T on the interaction length, in the vicinity of the mean-field point. We have encountered another avatar of the same paradox earlier, concerning the behaviour (4.19) of the velocity V right at the mean-field point. For generic values of the coupling constant ($g \neq 1$), the mean jamming time $\langle T \rangle$ is an *increasing* function of ξ_{int} , at least for a large enough system.

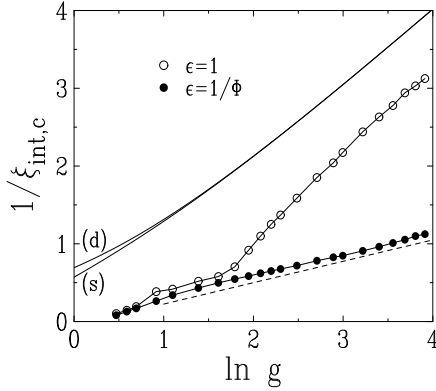


Fig. 9. Plot of $1/\xi_{\text{int},c}$ against $\ln g$, for both shape parameters $\varepsilon = 1$ and $\varepsilon = 1/\Phi$. The dashed line has slope 0.275. Upper full lines: static (s) and dynamical (d) thresholds for $\varepsilon = 1$.

As shown by (4.13), (4.15), and (4.16), it grows progressively as ξ_{int} increases in general: linearly in N in the ballistic phase, quadratically in N right at the critical point ($\xi_{\text{int}} = \xi_{\text{int},c}$), and exponentially in N in the activated phase. Right at the mean-field coupling ($g = 1$) however, the divergence law (4.19) of the velocity implies that $\langle T \rangle$ is a *decreasing* function of ξ_{int} . Far from being paradoxical, such behaviour is only to be expected; in general (far away from the mean-field coupling), an increase of ξ_{int} implies an increase of locally felt frustration, and jamming times are thereby increased. Right at the mean-field point however, there is in effect *no* local frustration, simply because the grains in the system are effectively non-interacting. In its immediate vicinity, an increased correlation length ξ_{int} implies that clusters of interacting grains of typical length ξ_{int} reorganise themselves collectively to reach a given ground state, so that the jamming time decreases with increasing ξ_{int} .

Figure 10 shows logarithmic plots of $\langle T \rangle$ against $g/(g+1)$ for $\varepsilon = 1/\Phi$. The data on the upper panel correspond to $N = 100$ and several values of ξ_{int} . The jamming time is observed to have a highly non-monotonic dependence on g . All the data start from the same value ($\langle T \rangle \approx 39$) in the $g \rightarrow 0$ limit. For $\xi_{\text{int}} = 1$ the data show a broad and shallow minimum. As ξ_{int} is increased, the data develop a clear minimum near the mean-field coupling ($g = 1$) and a maximum around $g \approx 0.3$. The maximum rises suddenly for $\xi_{\text{int}} \approx 35$, i.e., near the minimum value $\xi_{\text{int},c} \approx 36$ of the critical line, which is precisely reached for $g \approx 0.3$. The observed rise therefore corresponds to the crossover between the ballistic and activated phases. The data on the lower panel correspond to $\xi_{\text{int}} = \infty$, so that the system is in its extreme activated regime, except in the immediate neighborhood of the mean-field coupling $g = 1$. The observed irregularities are genuine, rather than being an artifact due to numerical noise; it was noticed that, if the column sizes were chosen to be successive Fibonacci numbers, the amount of irregularity could be kept to a minimum.

The data on the lower panel of Figure 10 show that the jamming time exhibits a dip around the mean-field

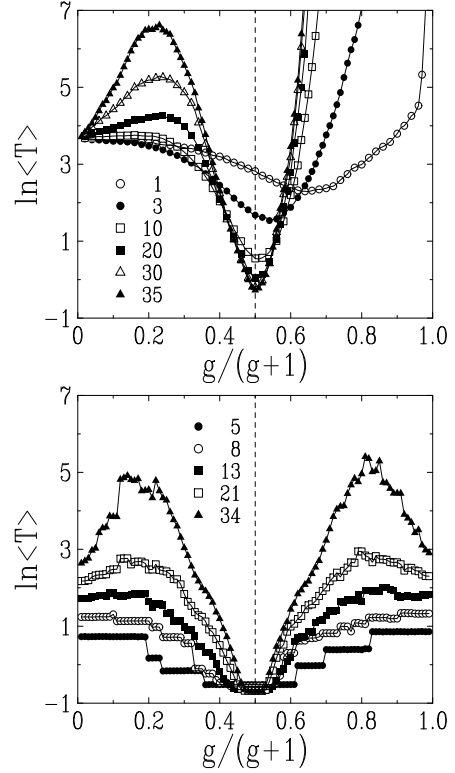


Fig. 10. Logarithmic plots of the mean jamming time $\langle T \rangle$ against $g/(g+1)$ for $\varepsilon = 1/\Phi$. Top: $N = 100$ and several values of ξ_{int} . Bottom: $\xi_{\text{int}} = \infty$ and column sizes equal to Fibonacci numbers from $F_5 = 5$ to $F_9 = 34$. Dashed lines: mean-field coupling ($g = 1$).

coupling ($g = 1$) in the $\xi_{\text{int}} = \infty$ limit, which gets more and more symmetric, deep and narrow as N is increased. The width of this dip can be measured by introducing two coupling constants $g_-(N) < 1 < g_+(N)$, one on either side of the mean-field point, such that $\langle T \rangle = 3$ (this value of the jamming time is chosen for convenience). Figure 11 shows a plot of the products $N^{1/2} \ln g_{\pm}(N)$ against $1/N$. Both sequences of coupling constants are observed to behave very symmetrically, and to depend on N in a very irregular way. The hulls of the data however converge to the non-trivial limits ± 1.75 , implying the scaling law

$$\delta g_+(N) \approx -\delta g_-(N) \sim N^{-1/2}. \quad (4.23)$$

We have indeed $\delta g = g - 1 \approx \ln g$ for $\delta g \ll 1$, in conformity with the ordinate of Figure 11.

The reason for the above scaling behaviour can be explained as follows. For $\xi_{\text{int}} = \infty$, the local field H_n acting on grain n reads

$$H_n = \eta - f(\sigma_n) + \delta g \sum_{m=n+1}^N f(\sigma_m), \quad (4.24)$$

where η is the mean field introduced in (3.11). In a random configuration of grain orientations, the difference $H_n - \eta$ can thus be evaluated to be of order $(\delta g)N^{1/2}$, by the

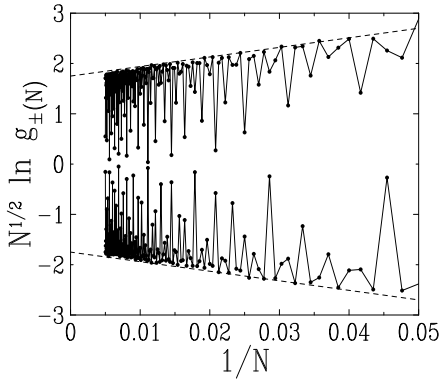


Fig. 11. Plot of the product $N^{1/2} \ln g_{\pm}(N)$ against $1/N$, where $g_{\pm}(N)$ are the two coupling constants such that $\langle T \rangle = 3$ for $\varepsilon = 1/\Phi$ and $\xi_{\text{int}} = \infty$. Upper data: $g_+(N) > 1$. Lower data: $g_-(N) < 1$. Dashed lines have intercepts ± 1.75 and slopes ± 19 .

law of large numbers. This estimate has two consequences. First, requiring that the difference $H_n - \eta$ is of order unity allows one to recover (4.23). Second, the above estimate can also be viewed as a finite-size scaling form of the result (4.20). The width $\delta g \sim N^{-1/2}$ of the dip is indeed expected to be such that ξ_{int} is comparable to N . This yields the quadratic divergence $\xi_{\text{int},c} \sim 1/(\delta g)^2$, as in (4.20).

Finally, the irregularities visible in the bottom panel of Figure 10, and especially in Figure 11, suggest an analogy with the phenomenon of defect nucleation, encountered in earlier work [12] to explain intermittency in the case of a weakly tapped ($\Gamma \ll 1$) column of irregular grains. Around the mean-field point, the predominant behaviour is of course dominated by the mean field; however, occasional perturbations in the form of excess j_n and h_n fields can lead to the nucleation of defects at specific sites n , generating the self-similar patterns observed.

Rôle of a finite ξ_{dyn}

So far we have limited the discussion of the dynamical phase diagram to the case where activation energies are negligible, so that $\xi_{\text{dyn}} = \infty$. The rôle of a finite dynamical length ξ_{dyn} has already been investigated in the $g \rightarrow 0$ regime for $\varepsilon = 1$ [13]. Its main effect is to induce two novel dynamical phases, whose main characteristics are as follows.

- *Logarithmic phase.* The logarithmic phase replaces the ballistic one for $\xi_{\text{int}} < \xi_{\text{int},c}$ when ξ_{dyn} is much smaller than N . In this regime, the system still orders from above, but the growth of the thickness $L(t)$ of the upper ordered layer is slowed down by gravity, according to the local frequencies (2.3). We have therefore

$$\frac{dL}{dt} \approx V \exp\left(-\frac{L}{\xi_{\text{dyn}}}\right). \quad (4.25)$$

The results (4.12) and (4.13) are recovered for $\xi_{\text{dyn}} \gg N$, i.e., in the ballistic phase. In the logarithmic phase, when

$\xi_{\text{dyn}} \ll N$, the thickness of the ordered layer is predicted to grow logarithmically:

$$L(t) \approx \xi_{\text{dyn}} \ln \frac{Vt}{\xi_{\text{dyn}}}, \quad (4.26)$$

so that the jamming time diverges exponentially fast:

$$\langle T \rangle \approx \frac{\xi_{\text{dyn}}}{V} \exp\left(\frac{N}{\xi_{\text{dyn}}}\right). \quad (4.27)$$

- *Glassy phase.* The glassy phase replaces the activated one when ξ_{dyn} is sufficiently small. The crossover between the activated and glassy phases takes place when the exponential growth of the slowest local time scale of the column, $1/\phi_N = e^{N/\xi_{\text{dyn}}}$ (which also governs the jamming time (4.27) in the logarithmic phase), exceeds the entropic growth $\langle T \rangle \sim e^{aN}$ characteristic of the activated phase. This line of reasoning predicts that the glassy phase can only be observed if ξ_{dyn} is a microscopic length: $\xi_{\text{dyn}} < 1/a$. The jamming time diverges exponentially with N in the glassy phase, according to $\langle T \rangle \sim e^{N/\xi_{\text{dyn}}}$.

Since the dependence on ξ_{dyn} remains unchanged with respect to the earlier case (see [13]), the purely depth-dependent features of the glassy and logarithmic phases remain the same. Among the novel features of the present model, we mention one related to the existence of a mean-field point.

Consider the model right at the mean-field coupling ($g = 1$). In the case of mean-field statics and slow dynamics, i.e., for $\xi_{\text{int}} = \infty$ and $N \gg \xi_{\text{dyn}}$, the jamming time grows exponentially with N , with an ε -dependent prefactor given by (4.8). In the generic situation where the column size N is much larger than both lengths ξ_{dyn} and ξ_{int} , the jamming time also grows exponentially with N , albeit with the ‘trivial’ prefactor of (4.27). Figure 12 presents a logarithmic plot of $\langle T \rangle$ against the ratio N/ξ_{dyn} , for $\varepsilon = 1/\Phi$, $g = 1$, $\xi_{\text{dyn}} = 50$, and several values of ξ_{int} . Both limiting growth rates are clearly observed, the crossover between both regimes occurring for very large values of ξ_{int} . We note again that the jamming time *decreases* with increasing ξ_{int} in the vicinity of the mean-field limit, consistent with the picture presented earlier. Finally, in order to avoid having large irregularities, N has been chosen to be a multiple of the Fibonacci number $F_{10} = 55$.

5 Dynamics: attractors

We next turn to the statistics of attractors sampled by zero-temperature dynamics, starting from a random initial configuration. This question is interesting because of its relationship with Edwards’ flatness hypothesis [18]; according to this, attractors are sampled uniformly, so that the static entropy Σ (see (3.8)) and the dynamical entropy S (see (4.10)) coincide.

For the time being, we consider the case where $\xi_{\text{dyn}} = \infty$. Attractor statistics have been investigated in [13] for $\varepsilon = 1$ in the $g \rightarrow 0$ limit, where ground states have a simple characterisation: they are all the dimerised configurations.

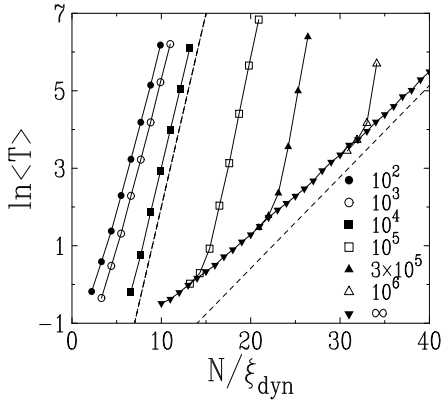


Fig. 12. Logarithmic plot of the mean jamming time $\langle T \rangle$ against the ratio N/ξ_{dyn} , for $\varepsilon = 1/\Phi$, $g = 1$, $\xi_{\text{dyn}} = 50$, and several values of ξ_{int} . The left dashed line has the unit slope corresponding to (4.27). The right one has the slope corresponding to (4.8), i.e., $(1 - \varepsilon)/(1 + \varepsilon) = 1/\Phi^3 \approx 0.236067$.

In the present case, for generic values of the parameters, the problem is more difficult because ground states are not known a priori, and most certainly do not allow for a simple static characterisation. In this respect the present situation is similar to that of tapping dynamics on various models, e.g. the Kob-Andersen model [21]. In the following we present data illustrating what are, according to us, the main features of the statistics of attractors.

First, in order to quantify the rôle of the coupling constant g , we have chosen to focus on the dynamical overlap between attractors $\sigma_n^{(g)}$ at coupling g and $\sigma_n^{(0)}$ at infinitesimal coupling ($g = 0^+$), defined as

$$\Omega = \frac{1}{N} \sum_{n=1}^N \langle \sigma_n^{(g)} \sigma_n^{(0^+)} \rangle. \quad (5.1)$$

Note that here the system is started in *the same* initial configuration and subjected to *the same* stochastic noise (i.e., in practice, the same sequence of random numbers).

Figure 13 shows data for Ω for $\varepsilon = 1$ and $\varepsilon = 1/\Phi$, $N = 50$ and 100 , and two values of the interaction length ($\xi_{\text{int}} = 3$ and 10) deep in the ballistic phase, i.e., much smaller than $\xi_{\text{int},c}$. The overlap behaves differently in both cases. For the irrational shape parameter $\varepsilon = 1/\Phi$ (top), the dynamics at infinitesimal coupling drive the system to its unique quasiperiodic ground state, so that Ω is nothing but the overlap between the finite-coupling attractor $\sigma_n^{(g)}$ and that ground state. This overlap exhibits a continuous decay as a function of g , which is remarkably size-independent. This suggests the following picture: quasiperiodic ordering spreads from the top of the column in the ballistic regime, as does the splitting of the quasiperiodic state into finite patches of length $L(g) \sim 1/g$ at finite coupling. For a given value of g , the orientation of a grain is fixed, depending on its position in one such patch. Increasing the length of the column leaves this orientation unchanged, only adding on more, similar patches corresponding to a given attractor, and thus leaving the over-

lap function unchanged. For the rational shape parameter $\varepsilon = 1$ (lower panel of Figure 13), the overlap behaves in a very different manner. It remains equal to unity in the range $0 < g < g_d$, where the values of the dynamical threshold g_d (see (4.18)) are shown as arrows. This is expected, as the dynamics are strictly independent of g in that range. The overlap then falls off very abruptly, more and more so for larger systems.

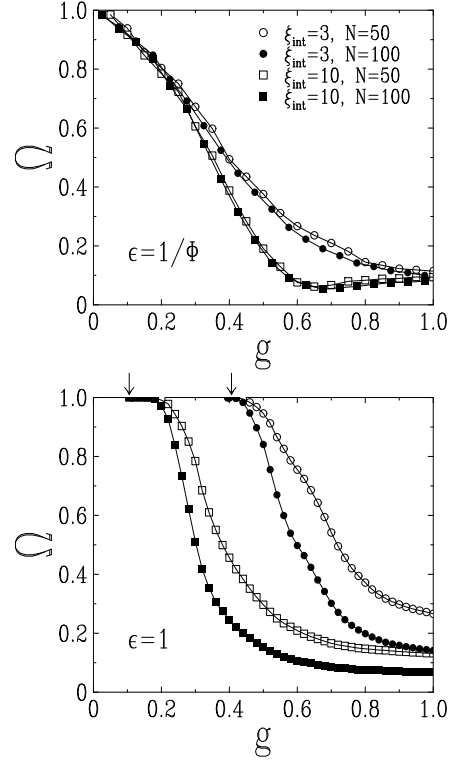


Fig. 13. Plot of the dynamical overlap Ω against g for both shape parameters $\varepsilon = 1/\Phi$ (top) and $\varepsilon = 1$ (bottom) and the same values of ξ_{int} and N . Arrows on top of the lower panel: dynamical threshold $g_d \approx 0.395612$ for $\xi_{\text{int}} = 3$ and $g_d \approx 0.105170$ for $\xi_{\text{int}} = 10$.

We now turn to the statistics of attractors *per se*. Let us first consider in detail the case $\varepsilon = 1$. In the weak-coupling phase ($0 < g < g_s$), attractors are known to consist of dimers. It is thus natural to characterise attractors by their contents in (polarised) dimers all over the phase diagram. The main difference between the present general situation and that of the weak-coupling regime is that now attractors are only *partially* dimerised. We are thus led to introduce *two* local dimer order parameters:

$$\Delta_k = -\langle \sigma_{2k-1} \sigma_{2k} \rangle, \quad \Pi_k = \frac{1}{2} \langle \sigma_{2k} - \sigma_{2k-1} \rangle. \quad (5.2)$$

The first order parameter is such that $\Delta_k = 1$ whenever there is a dimer at the k -th position and irrespective of its polarisation, whereas $\Delta_k = -1$ otherwise. The second one is sensitive to the polarisation of the dimer at the k -th position; it is such that $\Pi_k = +1$ if there is a $-+$ dimer,

$\Pi_k = -1$ if there is a $+-$ dimer, and $\Pi_k = 0$ otherwise. Both local order parameters vanish on average in a random configuration, where orientations are uncorrelated. Assuming that the column consists of an even number of grains ($N = 2K$), we also define global order parameters as spatial averages of the local ones:

$$\Delta = \frac{1}{K} \sum_{k=1}^K \Delta_k, \quad \Pi = \frac{1}{K} \sum_{k=1}^K \Pi_k. \quad (5.3)$$

The polarisation-sensitive order parameter Π_k can be recast in terms of the staggered orientation profile

$$S_n = (-1)^n \langle \sigma_n \rangle \quad (5.4)$$

as

$$\Pi_k = \frac{1}{2} (S_{2k} + S_{2k-1}), \quad (5.5)$$

so that

$$\Pi = \frac{1}{N} \sum_{n=1}^N S_n \quad (5.6)$$

is nothing but the mean staggered orientation.

Figure 14 shows a plot of the global dimer order parameter Δ of the attractors against g , for $\varepsilon = 1$, $N = 20$, and $\xi_{\text{int}} = 3$ and 10 . This modest system size has been chosen in order to test Edwards' flatness hypothesis fully. The plot indeed presents a comparison between (i) the static (or a priori) ensemble, where all attractors are obtained by means of an exact enumeration and taken with equal weights, and (ii) the dynamical ensemble, where attractors are sampled according to the dynamics, with a random initial configuration. Data pertaining to both ensembles behave similarly. They remain equal to unity in the whole range $0 < g < g_s$, where the values of the static threshold g_s (see (3.18)) are shown as arrows. Both datasets then fall off in a similar way (including their fine structure due to the finite size of the column), thus indicating that attractors are sampled rather uniformly by the dynamics. In other words, Edwards' hypothesis, although not exact, provides a good approximation to the attractor statistics in this ballistic regime.

Next, in order to investigate the possible consequences of slow (activated) dynamics on the statistics of attractors, we will deal with larger values of ξ_{int} and with arbitrary values of ε . A natural observable in this case [13] is the pseudo-energy \mathcal{E} per grain, defined as

$$\mathcal{E} = -\frac{1}{N} \sum_{n=1}^N H_n \sigma_n. \quad (5.7)$$

This definition can be motivated as follows. If the σ_n were independent spins in external fields H_n , (5.7) would be the corresponding Hamiltonian. In the present model, the local fields H_n depend on the orientations σ_m in a non-symmetric way, so that the dynamics do not obey detailed balance, and the statics are not described by a Hamiltonian. The pseudo-energy defined by (5.7) however provides a useful measure of the amount of disorder, either in an arbitrary configuration or in an attractor.

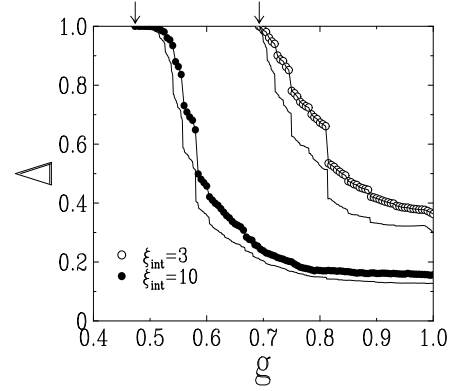


Fig. 14. Plot of the global dimer order parameter Δ of attractors against g for $\varepsilon = 1$, $N = 20$, and two values of ξ_{int} . Lines with symbols: dynamical ensemble. Lines without symbols: static ensemble. Arrows on top: static threshold $g_s \approx 0.692394$ for $\xi_{\text{int}} = 3$ and $g_s \approx 0.473376$ for $\xi_{\text{int}} = 10$.

We have chosen to focus on two values of the coupling constant, one on each side of the mean-field coupling, i.e., $g = 0.6$ and $g = 2$, where the critical value of the interaction length is respectively large and small. These are $\xi_{\text{int},c} \approx 51$ for $\varepsilon = 1$ and 48 for $\varepsilon = 1/\Phi$ when $g = 0.6$; and $\xi_{\text{int},c} \approx 5.2$ for $\varepsilon = 1$ and 5.9 for $\varepsilon = 1/\Phi$ when $g = 2$. Figure 15 shows plots of (minus) the mean pseudo-energy $\langle \mathcal{E} \rangle$ per grain against ξ_{int} in a range containing the critical values $\xi_{\text{int},c}$ (shown by arrows) which separate the ballistic and the activated phases. The mean energy exhibits a very weak and regular increase as a function of the interaction length ξ_{int} ; this verifies what we might expect, that increasing correlations will increase the amount of order in the system. The mean energy however, shows no anomalies at all as the critical point is crossed; this smooth behaviour is to be contrasted with the explosive rise in jamming times which accompanies it. Over the ranges of values of ξ_{int} corresponding to the plotted data, the mean jamming time indeed increases by factors of 150 for $\varepsilon = 1$ and 580 for $\varepsilon = 1/\Phi$ in the case of $g = 0.6$, and by factors of 2100 for $\varepsilon = 1$ and 80 for $\varepsilon = 1/\Phi$ in the case of $g = 2$.

Rôle of a finite ξ_{dyn}

The effect of a finite dynamical length ξ_{dyn} on the statistics of attractors has already been investigated in [13] for $\varepsilon = 1$ and $g \rightarrow 0$, that is, for weak frustration. The main qualitative conclusion there was that a truly non-trivial sampling of attractors was observed only in the glassy phase, whereas the attractor statistics in the three other dynamical phases were found to be in qualitative agreement with Edwards' flatness hypothesis. The effect of increasing frustration, in the present paper, might be expected only to enhance the non-triviality in the sampling of attractors in the glassy phase, thus deepening the contrast between this and the other three phases.

We consider first the vicinity of the mean-field point. Figure 16 shows the orientation profile $\langle \sigma_n \rangle$ of the attractors for parameters similar to those used in Figure 12,

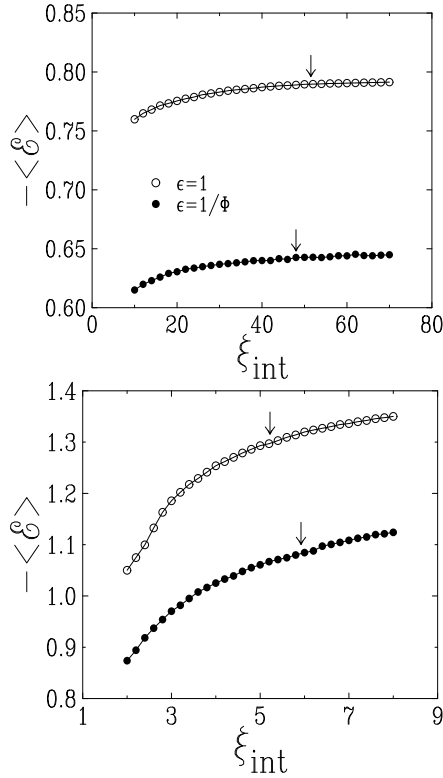


Fig. 15. Plot of (minus) the mean attractor pseudo-energy $\langle \mathcal{E} \rangle$ per grain against ξ_{int} , for $N = 200$ and both shape parameters. Arrows: critical values $\xi_{\text{int},c}$. Top: $g = 0.6$. Bottom: $g = 2$.

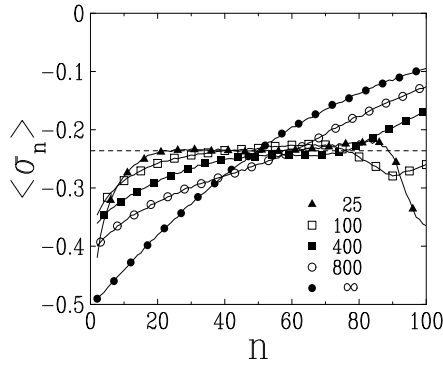


Fig. 16. Plot of the orientation profile of the attractors against depth n for $N = 100$, $\varepsilon = 1/\Phi$, at the mean-field coupling $g = 1$, and $\xi_{\text{dyn}} = 50$. Symbols: data for several values of ξ_{int} . Dashed line: mean orientation $\langle \sigma \rangle = -1/\Phi^3 \approx -0.236067$.

i.e., $\varepsilon = 1/\Phi$, $g = 1$, $N = 100$, and $\xi_{\text{dyn}} = 50$. In the case of mean-field statics ($\xi_{\text{int}} = \infty$), a non-trivial orientation profile is observed, similar to that shown in Figure 3. In the generic situation where the interaction length ξ_{int} is finite, the profile soon becomes very nearly flat, and therefore equal to its mean value (3.5), i.e., $\langle \sigma \rangle = -1/\Phi^3 \approx -0.236067$, thus indicating that attractors are sampled nearly uniformly by the dynamics.

Next, we explore the statistics of attractors for a generic coupling g , to, in particular, test the validity of Ed-

wards' hypothesis. We use a coupling constant greater than the mean field value ($g > 1$), so as to be able to have a relatively small $\xi_{\text{int},c}$ with our choice of boundary condition (4.1). The consequence of this is that the slow phases (activated and glassy) are easily observed with a modest system size. This possibility of tuning $\xi_{\text{int},c}$, and consequently system sizes, to reasonable values was not present in the case of the weak-coupling regime [13], where lengths were perforce large; it explains in part our rationale for not changing the boundary condition (4.1), of which more will be said in the concluding section.

We choose $\varepsilon = 1$, in order to keep using the local dimer order parameters (5.2), a coupling constant of $g = 2$, so that $\xi_{\text{int},c} \approx 5.2$, and a system size $N = 50$. We compare the nature of the attractors at $\xi_{\text{int}} = 2$ (below $\xi_{\text{int},c}$: ballistic to logarithmic crossover) and $\xi_{\text{int}} = 8$ (above $\xi_{\text{int},c}$: activated to glassy crossover). Figures 17 to 19 respectively show plots of the staggered orientation profile S_n and of the local dimer order parameter Δ_k and Π_k for several values of ξ_{dyn} spanning the crossovers.

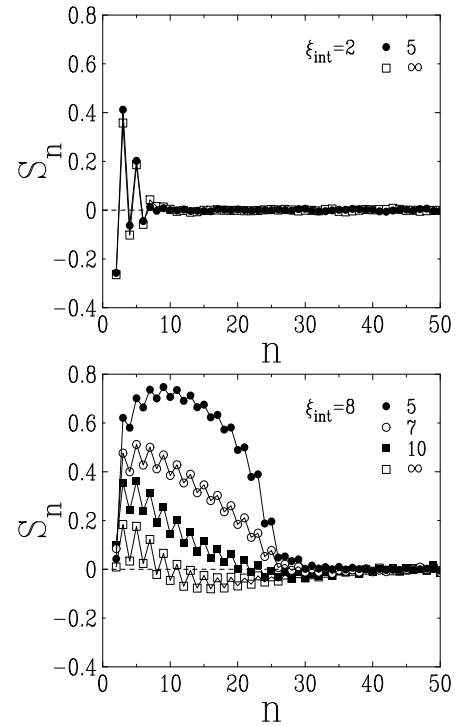


Fig. 17. Plot of the staggered orientation profile of the attractors against depth n for $\varepsilon = 1$, $g = 2$, $N = 50$, and several values of ξ_{dyn} . Top: $\xi_{\text{int}} = 2$. Bottom: $\xi_{\text{int}} = 8$.

Our earlier speculations are concretised by the following observations. The data for $\xi_{\text{int}} = 2$, shown in the upper panels of Figures 17 to 19, and pertaining to the crossover between the ballistic and the logarithmic phases, hardly show any dependence on ξ_{dyn} , i.e., on the fast (ballistic) or slow (logarithmic) nature of the dynamics. Since we have established that Edwards' flatness holds, at least qualitatively, for the ballistic phase, this is a clear indica-

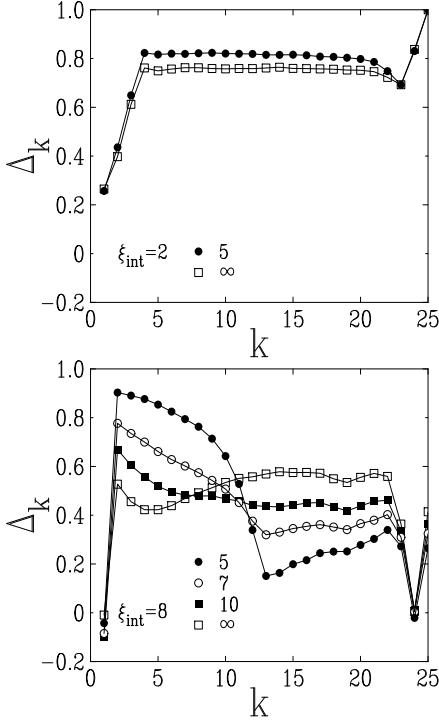


Fig. 18. Same as Figure 17 for the dimer order parameter Δ_k , plotted against the dimer number k .

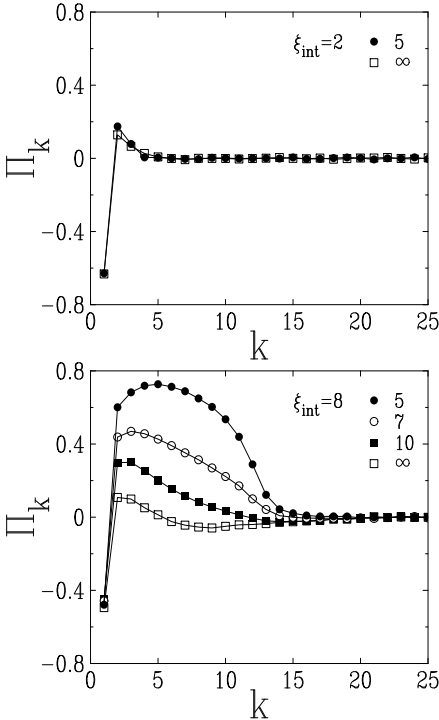


Fig. 19. Same as Figure 17 for the polarisation-sensitive dimer order parameter Π_k , plotted against the dimer number k .

tion that it holds also for the logarithmic phase. In terms of the actual ordering, we note the high and nearly uniform value of the dimer order parameter ($\Delta_k \approx 0.75$) in

the upper panel of Figure 18; the picture is that the attractor is most ordered at the base, and more or less ordered (dimerised) throughout its length, except near the very top. The staggered orientation profile and the order parameter Π_k , shown in the upper panels of Figures 17 and 19, demonstrate that the dimers are essentially unpolarised, except in a thin boundary layer near the top of the column.

On the other hand, the data for $\xi_{\text{int}} = 8$, shown in the lower panels of Figures 17 to 19, and pertaining to the crossover between the activated and the glassy phases, exhibit a strong dependence on ξ_{dyn} . Highly non-trivial profiles are observed for the smaller values of ξ_{dyn} , and especially for $\xi_{\text{dyn}} = 5$, which can be considered as glassy, given the modest size of the column. In this case, we see that the ensuing structure of the column is highly heterogeneous. The large values of the parameters Δ_k and Π_k observed in the upper part of the column indicate a large degree of dimerisation, most of the dimers being polarised as $-+$. In other words, there is a definite preference for *one* of the ‘crystalline’ arrangements of dimers found in earlier work [13] in the glassy regime for $\varepsilon = 1$ and $g \ll 1$. The choice of one preferred direction of polarisation can be explained as follows. The boundary condition $\sigma_1 = +1$, together with the observed smallness of $\langle \sigma_2 \rangle$, yields a definitely negative h_3 , and hence a trend toward $\langle \sigma_3 \rangle < 0$, i.e., $\Pi_2 > 0$. For $\xi_{\text{int}} = 8$ and $\xi_{\text{dyn}} = 5$, $\langle \sigma_2 \rangle \approx 0.04$ is indeed much smaller than $\langle \sigma_3 \rangle \approx -0.62$. The same polarising effect acts on the deeper dimers as well. Another notable difference with respect to the weak-coupling situation considered in [13] is that the lower part of the column appears much less ordered. One may speculate that a disordered lower part is a generic characteristic of attractors in the glassy regime. Grains are indeed very slow as soon as $n \gg \xi_{\text{dyn}}$, and thus hardly equilibrate. The weak-coupling regime for $\varepsilon = 1$ appears as an exception to this general rule, because there it is already known from statics that all ground states are fully dimerised.

6 Discussion

The full phase diagram of the frustrated column model has been presented in this work. This model of a column of grains has been developed [10] and investigated in earlier work, first in the directed situation ($g = 0$) for arbitrary values of the shape parameter ε [11,12], and then in the weak-coupling regime of the symmetric case ($\varepsilon = 1$, $g \ll 1$) [13]. The present work is the first investigation of the model over its entire parameter space, i.e., for generic values of ε , g , and of both lengths ξ_{int} and ξ_{dyn} . One of the most novel features is the existence of a mean-field point ($g = 1$) where the erstwhile local constraints on grain orientations disappear, becoming global; the model in this limit is similar to one of non-interacting grains, which has been analysed in [10].

The case of $\varepsilon = 1$ provides a useful illustration of many features of the model, including the physical nature of the mean-field limit. In this symmetric situation there are essentially two ways in which the average orientation of zero

can be achieved: by dimerised packings in the presence of strong local compacting constraints ($g \rightarrow 0$), and by uniformly random packings such that there are equal numbers of ordered and disordered grains globally, in the absence of local constraints ($g = 1$). Most of the features of the phase diagram for $\varepsilon = 1$ for $g < 1$ can be explained in terms of an interpolation between these two extremes. Beyond the mean-field limit ($g > 1$), the picture is one of a column of grains that is strongly frustrated, partly due to the chosen boundary condition (the uppermost spin is fixed), so that the activated phase extends down to arbitrary small values of ξ_{int} at strong coupling.

This is a natural point at which to discuss the implications of our choice (4.1) of boundary condition. For the directed model [11,12], where order propagated downwards, it was a natural choice to fix the top spin. This choice may seem to become less and less natural as increasing g , as the effects of the frustrating field j_n made the propagation of order less and less directional. Indeed, it might be argued that, in the large-coupling regime, the natural choice would be to fix the bottom spin, corresponding to the predominant upward propagation of order. There are two aspects to this issue. On the one hand, fixing the bottom spin rather than the top one might in fact make the phase diagram look more symmetric with respect to the weak-coupling end, and in particular show the explicit reappearance of the difference between regular and irregular grains in this. On the other hand, this would imply that we were replacing a fully frustrated column with a column where, instead, the ‘reverse’ field j_n could yield ballistic propagation until a finite $\xi_{\text{int},c}$ was reached – which is not physically correct. Thus our choice of fixing the top spin throughout the phase diagram has the advantage of retaining the sense of the interpolation from a fully directed model without frustration to the fully frustrated model for large g .

What can we predict experimentally for a box of grains? First, the ubiquity of our four phases (ballistic, logarithmic, activated and glassy) throughout the phase diagram (except at the mean-field point) vindicate our earlier picture [9] that the top of such a box would look ballistic, the middle activated and the bottom glassy. The relative sizes of the phases would of course vary depending on frustration: we might expect, given our study, that in the presence of strong frustration the size of the glassy phase would increase, and that of the ballistic one decrease. For timescales that are typical of experiment or simulation, we would see the highest fluctuations coming from the activated phase in the middle of a typical box [9]; however, for much longer times of observation, we would see large non-ergodic fluctuations at the bottom of the box, consistent with the glassy phase.

Finally, we predict that the effects of shape are most likely to be visible for very weak or very strong frustration, where there is a dominant propagation of order in our column in a given direction. In between them, when there is a balance between the propagation of order due to gravitational settling and that due to frustration, we

might expect shape effects to disappear as clusters of grains became the units of reorganisation.

References

1. A. Mehta, Soft Matter (Special Issue on Granular Media), DOI: 10.1039/b926809j (2010)
2. R.L. Brown and J.C. Richards, *Principles of Powder Mechanics* (Pergamon, New York, 1966)
3. K. To, P.Y. Lai, and H.K. Pak, Phys. Rev. Lett. **86**, 71 (2001); K. To, Phys. Rev. **E 71**, 060301 (R) (2005)
4. A. Mehta, G.C. Barker, and J.M. Luck, J. Stat. Mech. P10014 (2004); L.A. Pugnaloni, M. Mizrahi, C.M. Carlevaro, and F. Vericat, Phys. Rev. **E 78**, 051305 (2008); A. Garcimartin, I. Zuriguel, L.A. Pugnaloni, and A. Janda, arXiv:1005.5246v1 [cond-mat.soft]
5. D.M. Mueth, H.M. Jaeger, and S.R. Nagel, Phys. Rev. **E 57**, 3164 (1998); A. Tordesillas, J. Zhang, and R.P. Behringer, Geomech. Geoengin. **4**, 3 (2009); J. Zhang, T.S. Majmudar, A. Tordesillas, and R.P. Behringer, Granular Matter **12**, 159 (2010)
6. O. Dauchot, G. Marty, and G. Biroli, Phys. Rev. Lett. **95**, 265701 (2005); F. Lechenault, O. Dauchot, G. Biroli, and J.P. Bouchaud, Europhys. Lett. **83**, 46003 (2008)
7. H.C. Andersen, Proc. Natl. Acad. Sci. USA **102**, 6686 (2005); M.C. Jenkins and S.U. Egelhaaf, Adv. Colloid Interface Sci. **136**, 65 (2008); A. Widmer-Cooper, H. Perry, P. Harrowell, and D.R. Reichman, Nature Physics **4**, 711 (2008); D.J. Ashton and J.P. Garrahan, Eur. Phys. J. E **30**, 303 (2009); R.K. Darst, D.R. Reichman, and G. Biroli, J. Chem. Phys. **132**, 044510 (2010)
8. E.R. Nowak, J.B. Knight, E. Ben-Naim, H.M. Jaeger, and S.R. Nagel, Phys. Rev. **E 57**, 1971 (1998)
9. A. Mehta, G.C. Barker, and J.M. Luck, Proc. Natl. Acad. Sci. USA **105**, 8244 (2008)
10. P.F. Stadler, J.M. Luck, and A. Mehta, Europhys. Lett. **57**, 46 (2002)
11. A. Mehta and J.M. Luck, J. Phys. A **36**, L365 (2003)
12. J.M. Luck and A. Mehta, Eur. Phys. J. B **35**, 399 (2003)
13. J.M. Luck and A. Mehta, Eur. Phys. J. B **57**, 429 (2007)
14. G.W. Delaney and P.W. Cleary, Europhys. Lett. **89**, 34002 (2010)
15. M.E. Cates, J.P. Wittmer, J.P. Bouchaud, and P. Claudin, Phys. Rev. Lett. **81**, 1841 (1998)
16. A. Mehta, *Granular Physics* (Cambridge University Press, Cambridge, 2007)
17. S. Redner, *A Guide to First-Passage Processes* (Cambridge University Press, Cambridge, 2001)
18. S.F. Edwards, in *Granular Matter: An Interdisciplinary Approach*, edited by A. Mehta (Springer, New York, 1994)
19. S. Franz and M.A. Virasoro, J. Phys. A **33**, 891 (2000)
20. G. De Smedt, C. Godrèche, and J.M. Luck, Eur. Phys. J. B **27**, 363 (2002)
21. A. Barrat, J. Kurchan, V. Loreto, and M. Sellitto, Phys. Rev. Lett. **85**, 5034 (2000); Phys. Rev. **E 63**, 051301 (2001)